Bulletin of the Seismological Society of America, Vol. 92, No. 3, pp. 1015–1024, April 2002

Ⓔ

Ground Motions at Memphis and St. Louis from **M** 7.5–8.0 Earthquakes in the New Madrid Seismic Zone

by Gail M. Atkinson and Igor A. Beresnev

Abstract The New Madrid seismic zone is the most important regional seismic hazard in middle America, having produced several very large earthquakes in historic and geologic time. In this study we simulate time histories in Memphis, Tennessee, and St. Louis, Missouri, for **M** 7.5 and **M** 8.0 earthquakes along two faults in the New Madrid seismic zone. Simulations are based on a well-established and calibrated finite-fault simulation program (FINSIM), which has been shown to reproduce ground motions for earthquakes of **M** 4–8 in eastern and western North America (Beresnev and Atkinson, 2001a). Simulations are made for representative soil profiles for each city, as well as for reference bedrock conditions (at the base of the soil profile); the effect of nonlinearity on soil amplification is considered for the soil sites. Uncertainty in the results is considered by modeling a wide range of alternative scenarios, representing the major uncertainties in input parameters. The total uncertainty in ground motions (response spectra) is about a factor of 2. Results are most sensitive to magnitude, hypocenter location (directivity effects), and maximum slip velocity. The resulting time histories and spectra for all modeled scenarios are available as an electronic supplement to this article.

Results are validated to the extent possible using the modified Mercalli intensity (MMI) observations from the 1811–1812 earthquakes. The simulated motions are consistent with MMI observations at St. Louis and Memphis. It is not possible to distinguish, based on the MMI observations, which of the **M** 7.5 or **M** 8.0 scenarios are most likely. However, we conclude that the most extreme scenarios, such as **M** 8.0 with high slip velocity or large directivity effects, are not likely because they would produce higher MMI values than those that were observed.

Online material: time histories and spectra for modeled scenarios.

Introduction

An important problem in engineering seismology is the prediction of earthquake ground motions from future large earthquakes. Engineering analyses that assess the seismic performance of structures require seismological input that describes the amplitude, frequency content, and duration of the expected motions. This input generally takes the form of response spectra (for linear analyses) and time histories (for linear and nonlinear analyses) for selected scenario earthquakes that best represent the hazard at a site of interest. In the central United States the New Madrid seismic zone is the most important regional hazard, having produced several very large earthquakes in historic and geologic time. The size of the past earthquakes is not well constrained, being based on noninstrumental data (modified Mercalli intensity [MMI] data, limited geologic constraints, and paleoliquefaction features). The largest historical events, those from the 1811–1812 New Madrid sequence, are believed to be of moment magnitude (**M**) 7.5–8.0 (Johnston, 1996; Hough *et al.*, 2000). Earthquakes of this magnitude occur along the faults of the New Madrid seismic zone about every 450 yr (Schweig and Tuttle, 2000; Gomberg *et al.*, 2000). The large size and relatively frequent recurrence of New Madrid earthquakes make them particularly important scenario events for use in engineering analyses for cities in the Mississippi Embayment area.

In this study, we simulate time histories at Memphis, Tennessee, and St. Louis, Missouri, for **M** 7.5 and **M** 8.0 earthquakes along two faults in the New Madrid Seismic Zone (NMSZ); Memphis is about 60 km from the NMSZ, while the distance from the NMSZ to St. Louis is about 200 km. Simulations are based on a well-established and calibrated finite-fault simulation method (Beresnev and Atkinson, 1997, 1998a,b, 1999), which has been shown to reproduce ground motions for earthquakes of **M** 4–8 in eastern and western North America (Beresnev and Atkinson, 2001a). Simulations are made for representative soil profiles for each of the cities, as well as for reference bedrock conditions (at the base of the soil profile); the effect of nonlin-

earity on soil amplification is included for the soil sites. Uncertainty in the results is considered by modeling a wide range of alternative scenarios, representing the major uncertainties in input parameters. Results are validated to the extent possible using the modified Mercalli intensity (MMI) observations from the 1811–1812 earthquakes. The resulting time histories and spectra for all modeled scenarios are available as an electronic supplement to this article (*www.seismosoc.org*).

Simulation Model

Method

A discrete finite-fault model that captures the salient features of radiation from large earthquakes has been a popular seismological tool over the past two decades. As first introduced by Hartzell (1978), a finite-fault plane is subdivided into elements (subfaults), and radiation from a large earthquake is obtained as the sum of contributions from all elements, each of which acts as a small independent subsource. In the typical implementation, the rupture starts at a hypocentral point on the fault and propagates radially from it, triggering the subfaults as it passes them. The fields from all subevents are geometrically delayed and added together at the observation point. Engineering simulations of ground motions from significant seismic events have been performed primarily through such kinematic models (Kanamori, 1979; Irikura, 1983; Heaton and Hartzell, 1989; Somerville *et al.*, 1991; Hutchings, 1994; Tumarkin and Archuleta, 1994; Zeng *et al.*, 1994; see also the review in Beresnev and Atkinson, 1997).

In this study, we use the stochastic finite-fault simulation technique, which implements the concept of fault discretization wherein subevents are represented as stochastic point sources. The detailed description of the method is given by Beresnev and Atkinson (1997, 1998a); here we provide a general method outline. Every subfault is assigned an average ω^2 spectrum (eg., a Brune [1970, 1971] point-source spectrum) with a stochastic component superimposed on it. The stochastic component is needed to reproduce the random character of observed acceleration time histories. Rupture initiates at a specified subfault (hypocenter) and spreads radially outward along the fault plane at a specified rupture velocity, triggering each subfault as the rupture front passes its center. The number of subsources summed is prescribed by the total seismic moment of the target event. Even though each elementary source radiates an ω^2 spectrum, the result of the summation of all radiated fields under the conservation-of-total-moment constraint does not lead to the same spectral shape; a spectral sag is created by the summation process as previously described (also see Beresnev and Atkinson, 1999, pp. 609–610). The decay of spectral amplitudes with distance from the subsource to the site is given by a user-specified empirical function representing geometric and anelastic attenuation (whole path); the path component of the signal duration is also user specified. Amplification functions are specified to model the effect of amplification through the crustal velocity gradient (whole crust) and through the site-specific soil profile (near surface).

Beresnev and Atkinson (2001a,b) recently performed an extensive calibration of the method by modeling all well-recorded earthquakes of **M** 4–8 in eastern and western North America. This calibration established the average values and uncertainties of the two free parameters of the simulations: the maximum slip velocity (v_m) on the fault (which is directly proportional to the radiation strength factor parameter used in some of our previous articles, e.g., Beresnev and Atkinson, [1999] equation 4), and the subfault size (Δl). These two parameters control the amplitude of the simulated finite-fault spectrum at high and intermediate frequencies, respectively. When combined with the total moment of the simulated event, these parameters completely define the shape of the source spectrum. (Note: In our calibrated model the subevent stress drop is a fixed parameter that is used only to determine the moment associated with each subfault.) Beresnev and Atkinson (2001a) showed that these source model parameters are apparently region independent. For both eastern and western North America, the subfault size scales with magnitude, according to

$$\log\Delta l = -2 + 0.4\,\mathbf{M}, \quad 4 \le \mathbf{M} \le 8, \qquad (1)$$

where Δl is the subfault size in km. The maximum slip velocity is a stochastic variable whose average value is 0.45 m/sec; values typically range between 0.3 and 0.6 m/sec. There is some suggestion that lower slip velocities may be associated in general with larger-magnitude events (Beresnev and Atkinson, 2001a,b).

All simulations use the FORTRAN code FINSIM, which is freely available from the authors (Beresnev and Atkinson, 1998a).

Finite-Fault Model Parameters

The finite-fault simulations require specification of the fault-plane geometry, regional constants and attenuation parameters, and site-specific soil response information. The specific fault geometry of the 1811–1812 New Madrid earthquakes is not known, but the geologic structures along which the ruptures likely propagated have been studied (Johnston, 1996; Johnston and Schweig, 1996). The pattern of historical seismicity and focal mechanisms of modern events also suggests the trends and dimensions of the active structures. Figure 1 shows instrumental seismicity and two fault planes assumed for the simulations. The longer fault has a length (along strike) of 190 km and width (downdip) of 32 km, corresponding to an event of **M** 8.0, while the shorter fault has a length of 97 km and width of 22 km, corresponding to an event of **M** 7.5; the fault dimensions as a function of moment magnitude are based on the empirical relations of Wells and Coppersmith (1994) for fault length and fault area. The **M** 8 fault is assumed to follow the general trend of the Blytheville Arch–Bootheel lineament (Johnston and

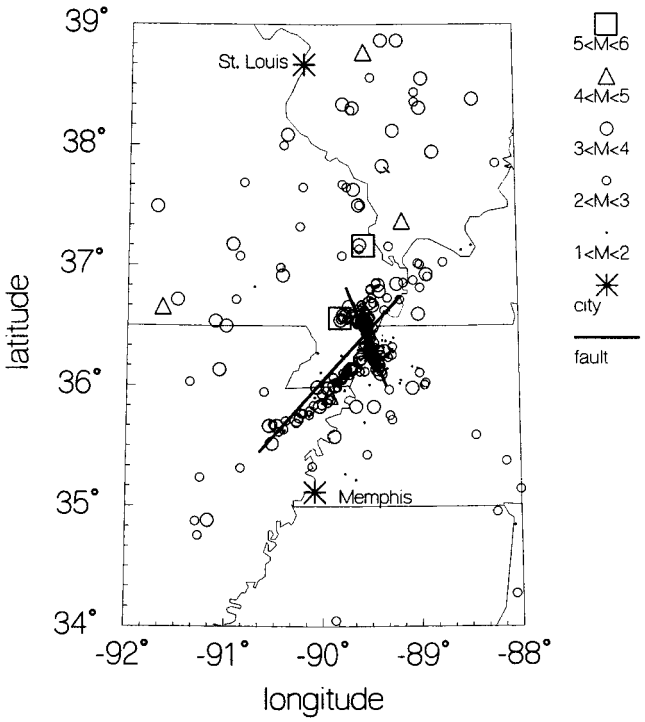

Figure 1. Map showing the fault locations and orientations for the simulations, along with earthquake locations for the period 1980–2000. Simulations are made for rock and soil sites at Memphis and St. Louis.

Table 1
New Madrid Finite-Fault Model Parameters: Rock Sites

Parameter	Parameter Value
M 8.0 fault geometry	Bootheel; strike = 220°; dip = 35°; L = 190 km; W = 32 km
M 7.5 fault geometry	Reelfoot; strike = 160°; dip = 70°; L = 97 km; W = 22 km
Depth to top of fault	1 km
$Q(f)$	$680f^{0.36}$
Geometric spreading	$1/R$ ($R \leq 70$ km) $1/R^{0}$ ($70 < R \leq 130$ km) $1/R^{0.5}$ ($R > 130$ km)
Distance-dependent duration term (sec)	0 ($R \leq 10$ km) 0.16 R ($10 < R \leq 70$ km) −0.03 R ($70 < R \leq 130$ km) 0.04 R ($R > 130$ km)
Crustal amplification	Boore-Joyner (1997) ENA
Bedrock kappa (sec)	0.002
Subfault stress parameter (bars)	50
Windowing function	Saragoni-Hart
Crustal shear-wave velocity (km/sec)	3.7
Rupture velocity	0.8 × (shear-wave velocity)
Crustal density (g/cm^3)	2.9
Fault-slip distribution	random
Maximum slip velocity (m/sec)	0.45
Stochastic trials to generate response spectrum	6

Schweig, 1996); it thus trends at 220° with a dip of 35° (mostly strike slip). The **M** 7.5 fault follows the Reelfoot Fault structure, with a strike of 160° and dip of 70° (Herrmann and Canas, 1978) (a thrust fault). Based on the lack of surface rupture, and the 900-m depth to Paleozoic rocks (Van Arsdale and TenBrink, 2000), the assumed minimum depth to the top of the fault surface is 1 km. The subfault size is specified according to equation (1). The maximum slip velocity is taken as the average value of 0.45 m/sec (radiation strength factor of 1.5).

The generic regional parameters that are fixed for all simulations are listed in Table 1. The attenuation and path effects are given by typical Q, geometric spreading, and distance-dependent duration operators for eastern North America, as well as the hard-rock kappa model (used just for rock simulations at the base of the soil profiles), all of which are taken from Atkinson and Boore (1995). These parameters were determined by empirical analysis of regional seismographic data in the northeastern United States and southeastern Canada (Atkinson and Mereu, 1992; Atkinson and Boore, 1995; Atkinson, 1996). A comparative study by the Electric Power Research Institute (1993) indicates that regional attenuation in the New Madrid area is not significantly different from that in the region studied by Atkinson and Mereu (1992); their attenuation model is generally applicable to most of eastern North America, including the New Madrid region. Physical constants are from Saikia and Somerville (1997) for the Mississippi Embayment region. Amplification through the crustal velocity gradient (e.g., from seismogenic depths to the base of the embayment soils) is as given by Boore and Joyner (1997) for the central United States.

The aforementioned parameters completely describe the simulation model for hard-rock sites. Hard-rock motions can be considered as input to the base of site-specific soil profiles. Alternatively, we can simulate motions for certain generic soil profiles by first finding the appropriate soil amplification function to be applied to the spectrum of the ground motion. The soil amplification function is then superimposed on the hard-rock regional crustal amplification to obtain total site amplification (e.g., total amplification is the product of the crustal amplification and the soil amplification functions).

Soil Amplification

Memphis and St. Louis are characterized by markedly different representative soil profiles, with soils at Memphis being deeper than those at St. Louis. We adopt the representative soil profile for each city as described by Wen and Wu (2001). These profiles are based on boring log data. The shear-wave velocity and density profiles are provided in Table 2. Site amplification occurs due to the combined effects

Table 2
Generic Soil Profiles*

Layer No.	Thickness (m)	Shear-Wave Velocity (m/sec)	Density (g/cm^3)
Memphis: kappa = 0.063			
1 (alluvium)	7	360	1.9
2 (alluvium)	5	360	2.0
3 (alluvium)	15	360	2.1
4 (loess)	9	360	2.2
5 (fluvial deposits)	8	360	2.0
6 (Jackson form.)	47	520	2.1
7 (Memphis sand)	246	667	2.3
8 (Wilex group)	83	733	2.4
9 (Midway group)	580	820	2.5
10 (Paleozoic rock)	500	3280	2.5
11	8000	3600	2.7
12	10000	3700	2.9
13	20000	4200	3.0
St. Louis: kappa = 0.0076			
1 (loess)	6	185	1.9
2 (glacio-fluvial)	10	310	2.1
3 (Miss. Limestone)	984	2900	2.6
4 (Paleozoic rock)	500	3280	2.5
5	8000	3600	2.7
6	10000	3700	2.9
7	20000	4200	3.0

*From Wen and Wu (2001), underlain by crustal model of Saikia and Somerville (1997).

of amplification through the velocity gradient (seismic impedance effect) and attenuation of high frequencies through energy absorption (kappa effect). The amplification effect is modeled using the well-known quarter-wavelength estimation method (Joyner and Fumal, 1985; Boore and Joyner, 1997). In this method, the amplification is given by

$$A = \sqrt{[(\rho_0\beta_0)/(\rho_s\beta_s)]}, \quad (2)$$

where ρ and β are the density and shear-wave velocity at the source (subscript 0) and site (subscript s). The site parameters are frequency dependent, as they are defined as the average velocity or density from the surface to a depth of a quarter wavelength. The amplification is counteracted by attenuation, described by the kappa operator (Anderson and Hough, 1984):

$$P = \exp(-\pi\kappa f), \quad (3)$$

where kappa (κ) accounts for damping within the soil profile. For Memphis and St. Louis, the kappa values deduced from seismographic recordings on soil sites are 0.063 and 0.0076 sec, respectively (Herrmann and Akinci, 1999). Figure 2 shows the combined effects of amplification and kappa for both cities, calculated using the quarter-wavelength amplification program of Boore (1996). The quarter-wavelength soil response estimate assumes entirely linear soil behavior.

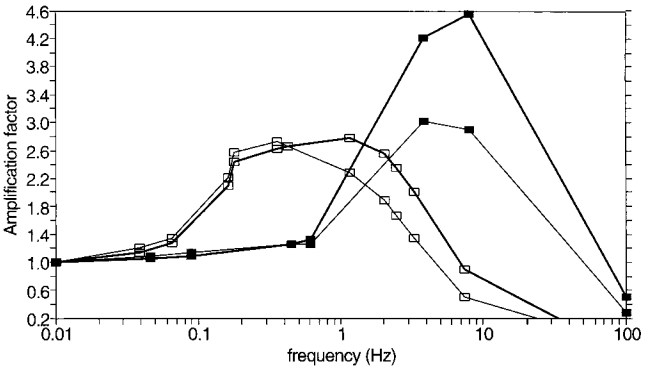

Figure 2. Amplification factors for the generic soil profiles (St. Louis, filled squares; Memphis, open squares). The upper line shows the linear amplification factor, including the effects of kappa, while the lower line shows the nonlinear amplification factor (for the **M** 8 event). The PGA_{rx} at the base of the soil profile for the **M** 8 event, which controls the degree of nonlinearity, is 232 cm/sec^2 at Memphis and 67 cm/sec^2 at St. Louis.

Treatment of Soil Nonlinearity

It is now well accepted that soils behave nonlinearly when subjected to strong levels of ground shaking (e.g., Beresnev and Wen, 1996; Field *et al.*, 1997, 1998; Beresnev *et al.*, 1998; Field and the SCEC Phase III Working Group, 2000). The effect of nonlinearity is to reduce the amount of amplification as the input ground-motion level is increased. Nonlinear soil effects can be assessed experimentally, analytically, or empirically. In this study, we use an empirical approach. The idea is to calculate the factor by which the computed soil amplification will be reduced by nonlinearity, as a function of input ground motion on rock. The factor is assessed by considering a range of empirical and analytical results. These results included (1) the empirical regression results of Abrahamson and Silva (1997), which give the nonlinear amplification of California soil sites relative to soft rock; (2) preliminary regression results from the global subduction database of Atkinson and Boore (2001), which can be used to infer linear and nonlinear amplification of soil sites relative to rock; and (3) the nonlinear amplification factors adopted by NEHRP (Borcherdt, 1995) based on a variety of studies. From these studies, we infer that the total soil amplification (S) of the response spectrum (pseudoacceleration, 5% damped, random horizontal component) at a given frequency can be described as

$$\log S = c_1 + c_2 \log(PGA_{rx}), \quad (4)$$

where PGA_{rx} is the predicted PGA on rock, in cm/sec^2, $c_2 = -0.0305 - 0.0841$ log(frequency), and c_1 represents the linear amplification factor, which depends on the soil type. The implied nonlinearity is similar to that of Abrahamson and Silva (1997) at low PGA (100 cm/s^2) and similar to that of NEHRP (Borcherdt, 1995) at high PGA (300 cm/s^2). We

use this result to calculate the amount by which to reduce the linear amplification determined for the three site profiles. Thus for each site we first calculate the motions input at the base of the soil layer, on hard rock. The nonlinear reduction factor (N) is then computed as:

$$\log N = c_2 \log(\mathrm{PGA}_{\mathrm{rx}}). \quad (5)$$

The net amplification effect for each soil profile is given by

$$S = APN, \quad (6)$$

where the functions A, P, and N are the frequency-dependent factors calculated from equations (2), (3), and (5), respectively. Figure 2 illustrates the nonlinear effect on the amplification, by showing the function S for the input ground motions for the **M** 8.0 and **M** 7.5 events, as well as for the linear case ($N = 1$).

There is considerable uncertainty in the deduced degree of nonlinearity, as it is derived from a variety of empirical analyses. Very deep soils, such as those found at Memphis, may not be well represented. For a very deep deposit, the lower part of the soil column would likely respond in a linear way, with nonlinearity being restricted to the upper 30 m or so. The PGA at the base of the nonlinear layer, as amplified by the lower (linear) portions of the soil profile, might thus be a more appropriate measure by which to judge nonlinearity. Our use of the PGA experienced at the base of the entire column as the reference level may underestimate the degree of nonlinearity, resulting in some unknown amount of conservatism in the estimated amplification. This potential source of conservatism is considered unimportant in view of other uncertainties.

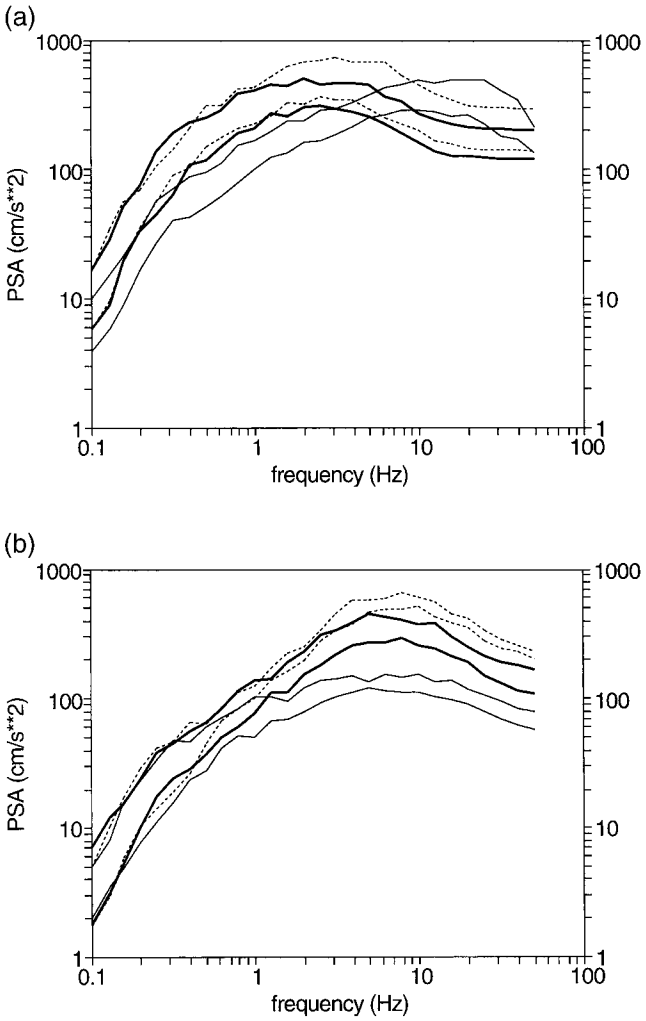

Figure 3. Average response spectra (log average over six trials) for **M** 7.5 and **M** 8.0 scenario events, assuming preferred (best-estimate) parameters. Light lines are motions on rock, at the base of the soil profile (lower line is **M** 7.5, upper line is **M** 8.0); dashed lines are motions that would be experienced on soil if the soil response was linear; heavy solid lines show motions considering the response of the soil to be nonlinear. PSA is 5% damped, random horizontal component pseudo-acceleration. (a) Memphis; (b) St. Louis.

Results and Discussion

Best Estimate Results

Using the stochastic finite-fault code FINSIM (Beresnev and Atkinson, 1998a) with the model parameters listed in Table 1, we generated six random horizontal components of motion at Memphis and St. Louis, for rock and generic soil conditions, for both of the postulated fault scenarios (**M** 8 Bootheel and **M** 7.5 Reelfoot). For these best-estimate scenarios, we assumed rupture initiation at the midpoint of the fault, thus providing a modest amount of directivity in both directions. Figure 3 shows the average response spectra for these scenarios at each city, for both rock and soil; in this figure we also show the result that is obtained if the soil is assumed to remain linear, so that the importance of the soil nonlinearity can be assessed. The linear soil results are obtained by assuming the net soil amplification $S = AP$, in place of the nonlinear case that assumes $S = APN$ (see equation 6). Sample time histories for soil sites are displayed in Figure 4 (all time histories are available in digital form from the electronic supplement); the high-frequency nature of the motions at St. Louis as compared to those at Memphis is apparent. This is due to the high-frequency site response attributable to the shallow generic soil profile at St. Louis. Figure 3 shows that the **M** 8.0 scenario results in motions about 1.5–2 times larger than the **M** 7.5 scenario. Expected motions in the 1-Hz frequency range are largest at Memphis, while high-frequency motions are largest at St. Louis. The effects of soil nonlinearity are quite important in reducing expected motions at high frequencies.

Alternative Scenarios

The ground motions that could result at any city from major New Madrid earthquakes are subject to large uncer-

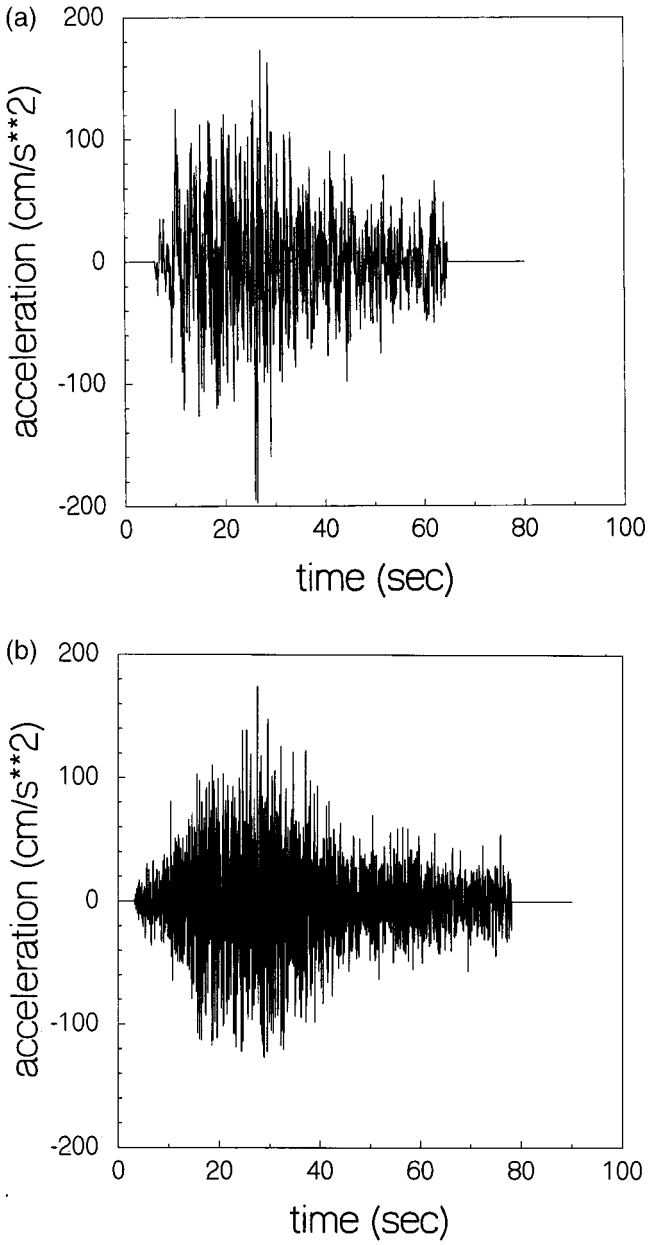

Figure 4. Example time histories on soil (including nonlinearity) for **M** 8.0 event. (a) Memphis; (b) St. Louis.

tainties due to parameter variability and uncertainty. In this section we explore the uncertainty of results by performing simulations for a range of plausible alternative scenarios. For each alternative scenario, we generate two random horizontal components of motion at each of the three cities, for both rock and soil (nonlinear). We consider variability in a single key parameter while holding all other parameters fixed at their best-estimate values. Thus this is an exercise in defining the sensitivity of results to plausible alternatives, rather than a logic-tree uncertainty analysis. A logic-tree approach could also be used but would not provide significant additional information, since there is little objective basis for estimating the full range or the likelihood of alternative parameters. The many thousand simulation cases that would be required to completely cover all parameter combinations are not warranted in this case. The following parameters are varied to estimate the uncertainty in results.

1. Hypocenter location: For each fault scenario, we consider a hypocenter at both the north and south ends of the fault. These alternatives provide for maximum directivity effects.
2. Fault strike: For the Bootheel **M** 8.0 fault, we consider a strike of 210°, which increases directivity effects toward Memphis, increasing motions there by about a factor of 2. Results at St. Louis are not much affected by this variability.
3. Maximum slip velocity: We consider maximum slip velocities that are about one standard deviation higher or lower than the assumed average value of 0.45 m/sec (ν_m = 0.3 m/sec, ν_m = 0.55 m/sec, corresponding to radiation strength factor of 1.0, 2.0). Since this parameter controls the strength of the high-frequency radiation, it has the most dramatic effect on the results. The largest amplitudes are obtained for an **M** 8 earthquake with ν_m = 0.55 m/sec, while the smallest amplitudes are obtained for the **M** 7.5 earthquakes with ν_m = 0.3 m/sec. The scenario involving a large magnitude with a high slip velocity is an extreme scenario that is rather implausible. The results of Beresnev and Atkinson (2001b) suggest that for large events, lower slip velocities are more likely. There is a poorly defined trend in inferred slip velocities from past earthquakes that suggests relatively low slip velocities for events of **M** ≥7.
4. Fault depth: Preliminary analyses indicated that the results are not sensitive to the location of the top of the fault plane; results are not significantly different if the top of the fault is assumed to be at 5-km depth rather than 1-km depth. This is not surprising given the large distance from the faults to the sites and the large dimensions of the fault planes.
5. Fault dip: Preliminary analyses indicated that the results are insensitive to reasonable variability in the assigned fault dip, so this parameter was not explored.

Figure 5 shows the range of response spectra obtained for the alternative scenarios previously described, in comparison to the best-estimate spectra. The figure shows results for the soil site conditions, for both cities. We infer that the total uncertainty in the results, including that due to variability in magnitude (7.5 or 8.0), is more than a factor of 2 but less than a factor of 3. For a given magnitude, the largest source of random variability is the hypocenter location (directivity) and the maximum slip velocity; these random variables produce an uncertainty of about a factor of 2.

An additional uncertainty that has not been considered is potential basin effects. Joyner (2000) showed that ground motions within deep sedimentary basins are elevated at long

periods (3 sec and greater), by as much as a factor of 3, due to the effect of surface waves propagating across the basin. This could affect motions at Memphis, which is located within the deep Mississippi Embayment. St. Louis is not within the basin, so basin effects are not a consideration there. During the 1991 **M** 4.6 Risco, Missouri, earthquake, a pronounced surface-wave train was observed at Memphis, consisting of Love waves of 3- to 5-sec period, and Rayleigh waves of 2- to 7-sec period (Dorman and Smalley, 1994). However, no such effect was observed during the 1990 **M** 4.8 Cape Girardeau, Missouri, earthquake. The Risco earthquake occurred within the basin, while the Cape Girardeau event was near the basin edge (Dorman and Smalley, 1994).

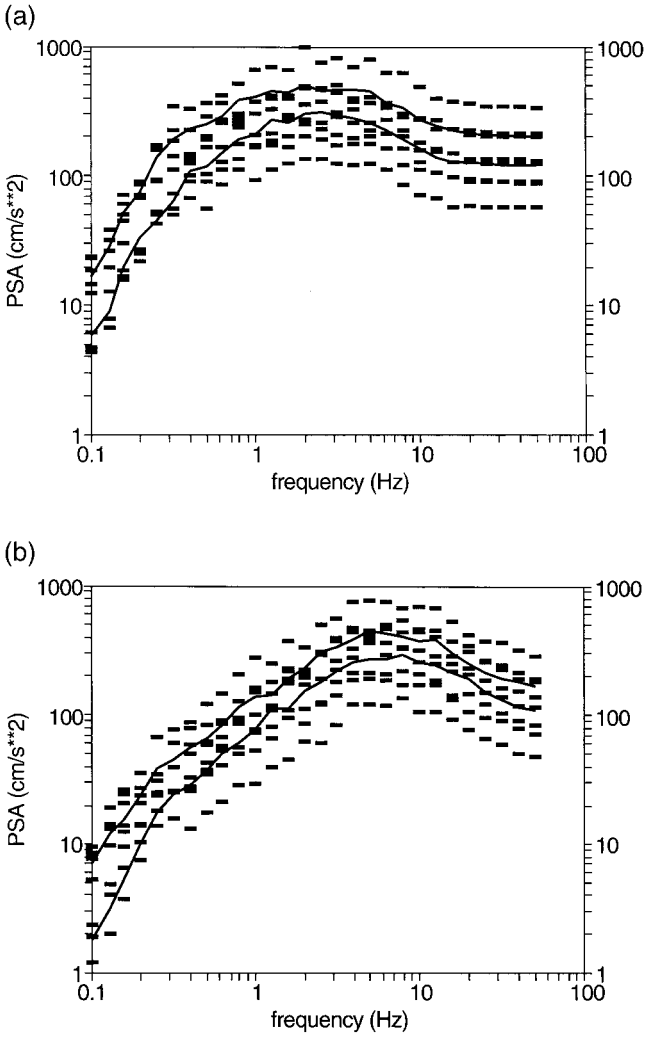

Figure 5. Sensitivity of response spectra to alternative input parameters, including variability in magnitude (7.5 or 8.0), hypocenter locations (directivity), fault strike, and maximum slip velocity. All spectra are for soil (nonlinear), 5% damped, horizontal component. Lines show spectra for preferred (best-estimate) input parameters for **M** 7.5 and 8.0, and symbols show values for alternative sets of input assumptions. (a) Memphis; (b) St. Louis.

Thus the generation of surface waves may depend on the location of the earthquake within the basin.

We consider the possible basin effects at Memphis as an additional amplification factor. Based on the empirical results presented by Joyner (2000), we postulate an additional amplification factor that has a value of 1.0 for frequencies of 1 Hz and greater. The amplification factor increases linearly with decreasing frequency from a factor of 1 at 1 Hz to a factor of 3 at frequencies of 0.33 Hz and less. Figure 6 shows the effects of this factor at Memphis for the **M** 8.0 and **M** 7.5 scenarios, relative to the other considered alternatives. The elevated long-period spectral content results in an amplified response over all frequencies. This happens because of the broadband nature of the response spectrum operator; an oscillator responds to a rather broad range of frequencies, especially those on the low side of the specified frequency. This representation of possible basin effects is only a crude approximation of a very complex phenomenon that could be explored in much greater detail. The point in presenting this comparison is to flag an issue that could be very important for long-period structures in Memphis, such as high-rise buildings or bridges.

Comparisons with Others

There are a few other studies of ground motions from New Madrid earthquakes against which the results of these simulations can be compared. Saikia and Somerville (1997) used a theoretical wave-propagation approach combined with empirical source parameters derived from the 1988 Saguenay, Quebec, earthquake to simulate ground motions on rock at St. Louis due to a **M** 7.5 New Madrid event. In Figure 7, we compare their spectra with our results for the best-estimate parameters for an event of **M** 7.5. Since the comparison is made for the generic soil site, we converted

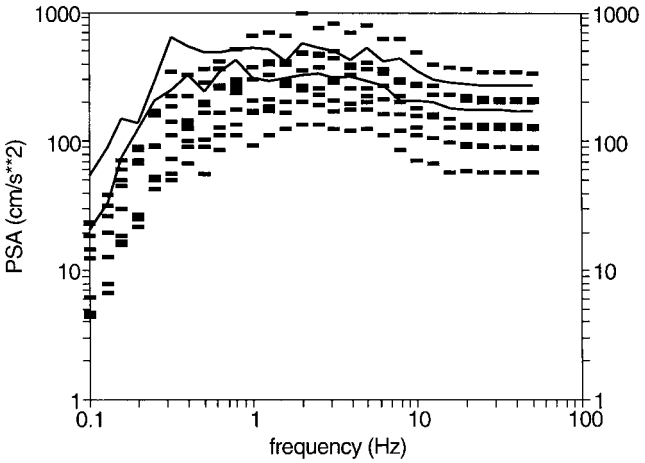

Figure 6. Possible basin effects on response spectra at Memphis. Symbols show range of alternative estimates (from Fig. 5a), and lines show spectra including an estimate of basin effects for **M** 7.5 and 8.0 events.

the Somerville and Saikia (1997) hard-rock result to our soil conditions by applying the identical soil factors that we used in our simulations. Our spectra are consistent in shape with those of Somerville and Saikia, but we obtain larger spectral amplitudes by about a factor of 2 overall. This reflects differences in the assumed attenuation and source parameters; attenuation differences may be very important because St. Louis is over 200 km from the source. Figure 7 also shows the spectrum obtained by Wen and Wu (2001) for the same generic soil profile that we used (recall that we adopted their generic soil profiles). The Wen and Wu study had a different focus in that it produced thousands of simulations to mimic a catalog of many years of earthquakes in the New Madrid seismic zone and the surrounding region. They included large New Madrid earthquakes and moderate local events to produce spectra having a 2% probability of exceedance in 50 yr. Their spectra are a composite of many different types of earthquakes, being dominated by large New Madrid earthquakes at low to intermediate frequencies but by moderate local events at high frequencies. Their 2% in 50 yr spectra for St. Louis are quite similar to our mean New Madrid spectra at low to intermediate frequencies (Note: Wen and Wu also used FINSIM to generate the New Madrid events but did not use the parameter constraints determined in our recent calibration studies). The Wen and Wu (2001) spectra exceed our New Madrid spectra at high frequencies, reflecting the influence of moderate local seismicity on the 2% in 50 yr spectra.

Seismic hazard at St. Louis and Memphis has recently been examined by Toro and Silva (2001). In their study, they define 2% in 50 yr spectra and specific earthquake scenarios that contribute to hazard in a specified frequency range. Their low-frequency scenario is a **M** 7.75 earthquake in the New Madrid seismic zone. For this scenario, they simulate ground motions for a range of site-specific generic soil profiles, using a stochastic point-source methodology. They include variability in the generic soil profile by considering three typical types of profiles for each location. Their spectra for this scenario event are compared to ours in Figure 8 for both St. Louis and Memphis. For this comparison, we have shown our mean spectrum, with plus or minus one standard deviation, as derived from a log average of the spectra from all of our alternative scenarios (including the best-estimate spectra). Overall, the results are quite comparable, despite the fact that Toro and Silva used a point-source model rather than the finite-fault approach used in our study. Toro and Silva obtain somewhat lower motions at high frequencies for St. Louis, mostly because of differences in the generic

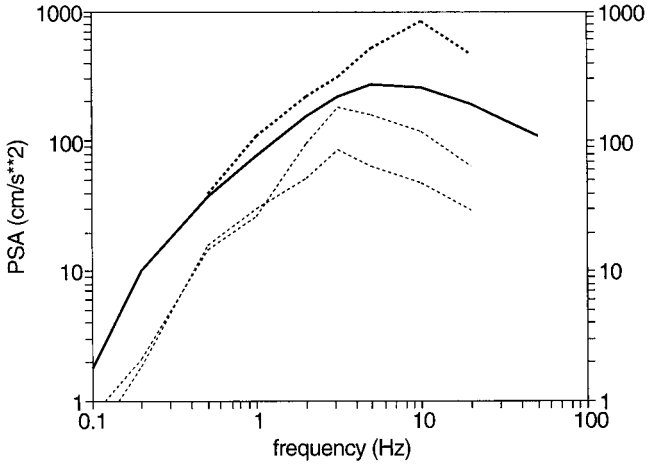

Figure 7. Comparison of the spectra of motions at St. Louis from this study with those of others. Solid line shows our best-estimate spectrum for **M** 7.5 event. Light dashed lines are the spectra of Saikia and Somerville (1997) for an event of **M** 7.5 (two horizontal components). Heavy dashed line is the 2% in 50 yr spectra of Wen and Wu (2001).

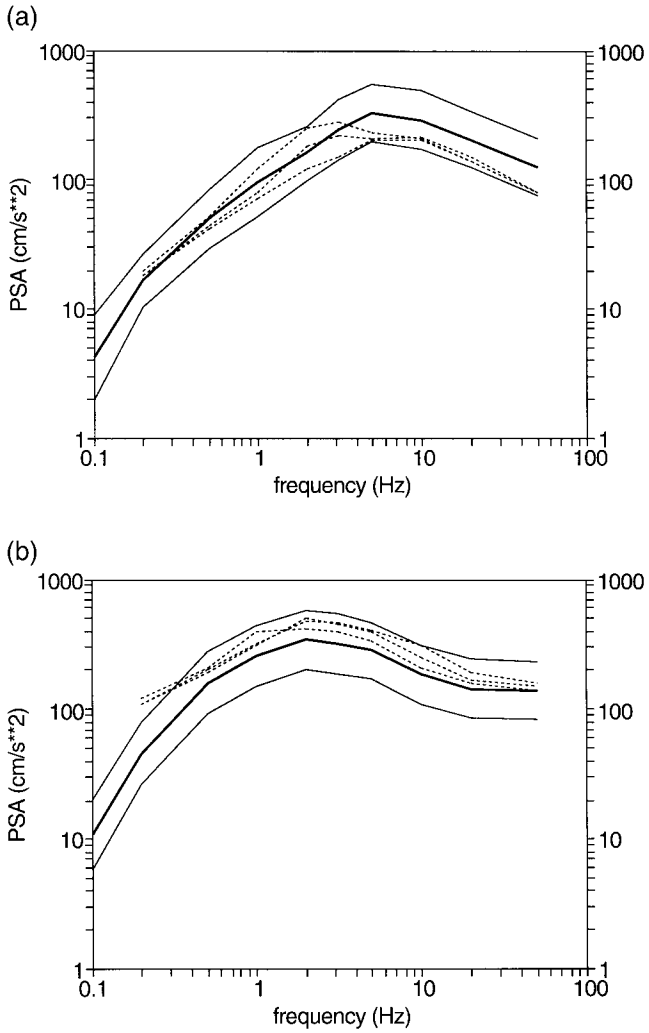

Figure 8. Comparison of the spectra of motions from this study with the **M** 7.75 scenario event spectra of Toro and Silva (2001). Solid line shows the mean and standard deviation of spectra (including all alternative input parameters) from this study. Dashed lines show the spectra of Toro and Silva for three alternative soil profiles. (a) St. Louis; (b) Memphis.

soil response (we infer high amplifications at high frequencies). At Memphis, the Toro and Silva results are higher at low frequencies. This is due to their point-source assumption, which considers an average effect of a Brune (single-corner) point-source model, and a double-corner point-source model (mimics finite-fault) (see Beresnev and Atkinson [1999, 2001b] for a discussion of the single-corner and double-corner point-source models in relation to the finite-fault model). Overall, we conclude that the results of this study are consistent with previous investigations but provide more detail on the range of time histories to be expected at St. Louis and Memphis due to large scenario earthquakes in the New Madrid seismic zone.

Comparisons with MMI Observations

Validation of ground-motion predictions using empirical observations is an important and necessary component of any simulations to be used for engineering purposes. Our overall technique has been validated against previous large earthquakes in both eastern and western North America (Beresnev and Atkinson, 2001a,b), but an examination of the predictions with respect to observations from the 1811–1812 New Madrid earthquakes is most relevant. Therefore the spectra of this study are assessed in relation to the 1811–1812 MMI observations. As described by Atkinson (2001), a response spectrum can be used to estimate the MMI value that it would be expected to produce, based on empirical correlations between MMI and PSA drawn from the California database (Atkinson and Sonley, 2000). An expected MMI value is obtained by averaging inferred MMI values over the 1- to 10-Hz frequency range, as obtained from the empirical correlations of Atkinson and Sonley (2000). The results are summarized in Table 3. The observed MMI is taken from information provided by Hough *et al.* (2000) for the largest of the three shocks (not necessarily the same shock at each city), including some uncertainty due to conflicting reports where applicable. It is concluded that the observed MMI of 7–8 at St. Louis is consistent with the **M** 7.5 or **M** 8.0 best-estimate scenarios or the average of the alternative scenarios. However, the lowest of the alternative estimates would underestimate MMI at St. Louis, while the highest of the alternatives would overestimate it. At locations near the present-day Memphis, the observed MMI of 8 is most consistent with the **M** 8.0 scenarios, although **M** 7.5 scenarios cannot be excluded due to uncertainty. We conclude that the more extreme of the alternative scenarios, at both the high and low ends of the range, are unlikely based on the MMI data.

Table 3
Comparison of MMI Inferred from Simulations with Observed MMI from 1811–1812 New Madrid Earthquakes

City	Observed MMMI	Best **M** 8.0 Scenario	Best **M** 7.5 Scenario	Average All Cases	Mean + Std. Deviation	Mean − Std. Deviation
St. Louis	7 to 8	8	7	8	6	9
Memphis	8	8	7	7	5	8

Conclusions

We have simulated time histories at St. Louis and Memphis for scenario earthquakes of **M** 7.5 to 8.0 on the faults of the New Madrid seismic zone. These time histories, which may be downloaded from the electronic supplement, may be used to assess the performance of structures to future large earthquakes. The uncertainty in ground motions due to uncertainty in the input parameters of the simulations is about a factor of 2. The simulated motions are consistent with MMI observations. It is not possible to distinguish, based on the MMI observations, which of the **M** 7.5 or **M** 8.0 scenarios are most likely. However, we conclude that the most extreme scenarios, such as **M** 8.0 with high slip velocity or large directivity effects, are not likely because they would produce higher MMI values than those that were observed.

Acknowledgments

This study was funded by the National Earthquake Hazards Reduction Program, under Grant 99HQGR0027. We thank Bob Herrmann for constructive comments that improved the manuscript.

References

Abrahamson, N., and W. Silva (1997). Empirical response spectral attenuation relations for shallow crustal earthquakes, *Seism. Res. Lett.* **68,** 94–127.

Anderson, J., and S. Hough (1984). A model for the shape of the Fourier amplitude spectrum of acceleration at high frequencies, *Bull. Seism. Soc. Am.* **74,** 1969–1993.

Atkinson, G. (1996). The high-frequency shape of the source spectrum for earthquakes in eastern and western Canada, *Bull. Seism. Soc. Am.* **86,** 106–112.

Atkinson, G. (2001). Linking historical intensity observations with ground motion relations for eastern North America, *Seism. Res. Lett.* **72,** 560–574.

Atkinson, G., and D. Boore (1995). New ground motion relations for eastern North America, *Bull. Seism. Soc. Am.* **85,** 17–30.

Atkinson, G., and D. Boore (2001). Preliminary ground motion relations for subduction zone earthquakes, *Seism. Res. Lett.* **72,** 282.

Atkinson, G., and R. Mereu (1992). The shape of ground motion attenuation curves in southeastern Canada, *Bull. Seism. Soc. Am.* **82,** 2014–2031.

Atkinson, G., and E. Sonley (2000). Empirical relationships between modified Mercalli intensity and response spectra, *Bull. Seism. Soc. Am.* **90,** 537–544.

Beresnev, I. A. (2002). Nonlinearity at California generic soil sites from modeling recent strong-motion data, *Bull. Seism. Soc. Am.* (in press).

Beresnev, I., and G. Atkinson (1997). Modeling finite fault radiation from the ω*n* spectrum, *Bull. Seism. Soc. Am.* **87,** 67–84.

Beresnev, I., and G. Atkinson (1998a). FINSIM: a FORTRAN program for simulating stochastic acceleration time histories from finite faults, *Seism. Res. Lett.* **69,** 27–32.

Beresnev, I., and G. Atkinson (1998b). Stochastic finite-fault modeling of ground motions from the 1994 Northridge, California earthquake. I. Validation on rock sites, *Bull. Seism. Soc. Am.* **88,** 1392–1401.

Beresnev, I., and G. Atkinson (1999). Generic finite-fault model for ground-motion prediction in eastern North America, *Bull. Seism. Soc. Am.* **89,** 608–625.

Beresnev, I., and G. Atkinson (2001a). Subevent structure of large earthquakes: a ground motion perspective, *Geophys. Res. Lett.* **28,** 53–56.

Beresnev, I., and G. Atkinson (2001b). Source parameters of earthquakes in eastern and western North America based on finite-fault modeling, *Bull. Seism. Soc. Am.* (in press).

Beresnev, I., and K.-L. Wen (1996). Nonlinear soil response: a reality? *Bull. Seism. Soc. Am.* **86,** 1964–1978.

Beresnev, I. A., G. M. Atkinson, P. A. Johnson, and E. H. Field (1998). Stochastic finite-fault modeling of ground motions from the 1994 Northridge, California, earthquake. II. Widespread nonlinear response at soil sites, *Bull. Seism. Soc. Am.* **88,** 1402–1410.

Boore, D. (1996). SMSIM: Fortran programs for simulating ground motions from earthquakes, *U.S. Geol. Surv. Open-File Rept. 96-80-A.*

Boore, D., and W. Joyner (1997). Site amplifications for generic rock sites, *Bull. Seism. Soc. Am.* **87,** 327–341.

Borcherdt, R. (1995). Estimates of site-dependent response spectra for design, *Earthquake Spectra* **10,** 617–654.

Brune, J. (1970). Tectonic stress and the spectra of seismic shear waves from earthquakes, *J. Geophys. Res.* **75,** 4997–5009.

Brune, J. (1971). Correction, *J. Geophys. Res.* **76,** 5002.

Dorman, J., and R. Smalley (1994). Low-frequency seismic surface waves in the New Madrid zone, *Seism. Res. Lett.* **65,** 137–148.

Electric Power Research Institute (1993). *Guidelines for Determining Design Basis Ground Motions: Early Site Permit Demonstration Program*, Electric Power Research Institute, Palo Alto, California, Vol. 1, RP3302.

Field, E. H., and the SCEC Phase III Working Group (2000). Accounting for site effects in probabilistic seismic hazard analyses of southern California: overview of the SCEC Phase III Report, *Bull. Seism. Soc. Am.* **90,** S1–S31.

Field, E. H., P. A. Johnson, I. A. Beresnev, and Y. Zeng (1997). Nonlinear ground-motion amplification by sediments during the 1994 Northridge earthquake, *Nature* **390,** 599–602.

Field, E. H., S. Kramer, A.-W. Elgamal, J. D. Bray, N. Matasovic, P. A. Johnson, C. Cramer, C. Roblee, D. J. Wald, L. F. Bonilla, P. P. Dimitriu, and J. G. Anderson (1998). Nonlinear site response: where we're at, *Seism. Res. Lett.* **69,** 230–234.

Gomberg, J., G. Atkinson, W. Bakun, P. Bodin, D. Boore, C. Cramer, A. Frankel, P. Gasperini, T. Hanks, B. Herrmann, S. Hough, A. Johnston, S. Kenner, C. Langston, M. Linker, P. Mayne, M. Petersen, C. Powell, W. Prescott, E. Schweig, P. Segall, S. Stein, B. Stuart, M. Tuttle, and R. VanArsdale (2000). Reassessing the New Madrid Seismic Zone, *EOS* **81,** no. 35, 397, 402–403.

Hartzell, S. (1978). Earthquake aftershocks as Green's functions, *Geophys. Res. Lett.* **5,** 1–14.

Heaton, T., and S. Hartzell (1989). Estimation of strong ground motions for hypothetical earthquakes on the Cascadia subduction zone, Pacific Northwest, *Pure Appl. Geophy.* **129,** 131–201.

Herrmann, R., and A. Akinci (1999). Mid-America ground motion models, *http://www.eas.slu.edu/People/RBHerrmann/MAEC/maecgnd.html* (last accessed 16 January 2002).

Herrmann, R., and J. Canas (1978). Focal mechanism studies in the New Madrid seismic zone, *Bull Seism. Soc. Am.* **68,** 1095–1102.

Hough, S., J. Armbruster, L. Seeber, and J. Hough (2000). On the modified Mercalli intensities and magnitudes of 1811–1812 New Madrid earthquakes, *J. Geophys. Res.* **105,** 839–864.

Hutchings, L. (1994). Kinematic earthquake models and synthesized ground motion using empirical Green's functions, *Bull. Seism. Soc. Am.* **84,** 1028–1050.

Irikura, K. (1983). Semi-empirical estimation of strong ground motions during large earthquakes, *Bull. Dis. Prev. Res. Inst. Kyoto Univ.* **33,** 63–104.

Johnston, A. (1996). Seismic moment assessment of earthquakes in stable continental regions. III. *Geophys. J. Int.* **126,** 314–344.

Johnston, A., and E. Schweig (1996). The enigma of the New Madrid earthquakes of 1811–1912, *Annu. Rev. Earth Planet Sci.* **24,** 339–384.

Joyner, W. (2000). Strong motion from surface waves in deep sedimentary basins, *Bull. Seism. Soc. Am.* **90,** S95–S112.

Joyner, W., and T. Fumal (1985). Predictive mapping of ground motion in *Evaluating Earthquake Hazards in the Los Angeles Region,* Ziony (Editor), *U.S. Geol. Surv. Prof. Pap. 1360,* 203–220.

Kanamori, H. (1979). A semi-empirical approach to prediction of long-period motions from great earthquakes, *Bull. Seism. Soc. Am.* **69,** 1645–1670.

Saikia, C., and P. Somerville (1997). Simulated hard-rock motions in Saint Louis, Missouri, from large New Madrid earthquakes ($M_W \geq 6.5$), *Bull. Seism. Soc. Am.* **87,** 123–139.

Schweig, E., and M. Tuttle (2000). *Proc. of USGS Workshop on New Madrid Source Characterization,* Memphis, Tennessee, 20–21 January 2000 (*www.ceri.memphis.edu/usgs/hazmap/20jan00minutes.shtml*).

Somerville, P., M. Sen, and B. Cohee (1991). Simulations of strong ground motions recorded during the 1985 Michoacan, Mexico, and Valparaiso, Chile, earthquakes, *Bull. Seism. Soc. Am.* **81,** 1–27.

Toro, G., and W. Silva (2001). *Scenario Earthquakes for Saint Louis, MO and Memphis, TN, and Seismic Hazard Maps for the Central United States Region Including the Effect of Site Conditions,* Risk Engineering, Boulder, Colorado (*www.riskeng.com*).

Tumarkin, A. G., and R. J. Archuleta (1994). Empirical ground motion prediction, *Ann. Geofis.* **37,** 1691–1720.

Van Arsdale, R., and R. TenBrink (2000). Late Cretaceous and Cenozoic geology of the New Madrid Seismic Zone, *Bull. Seism. Soc. Am.* **90,** 345–356.

Wells, D., and K. Coppersmith (1994). New empirical relationships among magnitude, rupture length, rupture width, rupture area, and surface displacement, *Bull. Seism. Soc. Am.* **84,** 974–1002.

Wen, Y., and C. Wu (2001). Uniform hazard ground motions for mid-America cities, *Earthquake Spectra* **17,** 359–384.

Zeng, Y, J. G. Anderson, and G. Yu (1994). A composite source model for computing realistic strong ground motions, *Geophys. Res. Lett.* **21,** 725–728.

Dept. Earth Sciences
Carlton University
Ottawa, Ontario, Canada K1S 5B6
gma@ccs.carleton.ca
(G.M.A.)

Dept. Earth Sciences
Iowa State University
Ames, Iowa
beresnev@iastate.edu
(I.A.B.)

Manuscript received 20 July 2001.